land

MDPI

Article

Multi-Ecohydrological Interactions Between Groundwater and Vegetation of Groundwater-Dependent Ecosystems in Semi-Arid Regions: A Case Study in the Hailiutu River Basin

Lei Zeng [1,2,3,4,†], Li Xu [5,6,*,†], Boying Song [5,6], Ping Wang [5,6], Gang Qiao [1,2,3,4], Tianye Wang [7], Hu Wang [1,2,3,4] and Xuekai Jing [1,2,3,4]

1 Xi'an Center of China Geological Survey, Ministry of Natural Resources, Xi'an 710019, China; zlei@mail.cgs.gov.cn (L.Z.); qgang@mail.cgs.gov.cn (G.Q.); whu02@mail.cgs.gov.cn (H.W.); jxuekai@mail.cgs.gov.cn (X.J.)
2 Observation and Research Station of Groundwater and Ecology in Yulin, Shaanxi, Ministry of Natural Resources, Yulin 710019, China
3 Key Laboratory for Groundwater and Ecology in Arid and Semi-arid Areas, China Geological Survey, Xi'an 710019, China
4 Shaanxi Water Resources and Environment Engineering Technology Research Center, Xi'an 710019, China
5 Key Laboratory of Water Cycle and Related Land Surface Processes, Institute of Geographic Sciences and Natural Resources Research, Chinese Academy of Sciences, Beijing 100101, China; sby17337997960@163.com (B.S.); wangping@igsnrr.ac.cn (P.W.)
6 University of Chinese Academy of Sciences, Beijing 100049, China
7 School of Water Conservancy and Transportation, Zhengzhou University, Zhengzhou 450001, China; wangtianye@zzu.edu.cn
* Correspondence: xuli241@mails.ucas.ac.cn
† These authors contributed equally to this work.

Abstract

The Hailiutu River Basin in northern China represents a semi-arid area where groundwater-dependent ecosystems (GDEs) play a critical role in maintaining regional vegetation structure and ecological stability. This study investigated the spatiotemporal dynamics of GDEs and their relationship with water conditions using trend analysis, partial correlation, and Random Forest models over the period of 2002–2022. The results show that vegetation activity (NDVI) increased at a rate of 0.0052/yr in GDEs. Precipitation exhibited a basin-wide upward trend of 0.735 mm/yr, while SPEI increased at 0.0207/yr. In contrast, groundwater storage declined markedly at −11.19 mm/yr, highlighting a persistent reduction in water availability that poses a significant risk to the stability of GDEs. Both partial correlation analysis and the random forest model consistently showed strong ecohydrological interactions between vegetation and groundwater. Vegetation dynamics are primarily driven by groundwater availability, especially in groundwater-dependent ecosystems. Conversely, groundwater variations are most strongly influenced by vegetation. The results indicate that precipitation and the standardized precipitation–evapotranspiration index (SPEI) are the primary positive drivers of interannual NDVI variability, whereas groundwater plays a critical role in sustaining GDEs. Field observations of key species confirm the dependence of GDEs on groundwater, and vegetation dynamics are regulated by climate and groundwater; however, ongoing groundwater decline may threaten ecosystem stability. These findings demonstrate that vegetation transpiration exerts the dominant influence on groundwater variations, while groundwater simultaneously constrains vegetation growth, particularly in areas where declining groundwater storage anomalies (GWSAs) coincide with reduced NDVI. The results emphasize that continuous groundwater depletion threatens vegetation–groundwater sustainability, highlighting the need for balanced groundwater and vegetation management in arid regions.

Check for updates

Academic Editors: Nunziarita Palazzolo and Luca Furnari

Received: 16 October 2025
Revised: 18 December 2025
Accepted: 22 December 2025
Published: 29 December 2025

Copyright: © 2025 by the authors. Licensee MDPI, Basel, Switzerland. This article is an open access article distributed under the terms and conditions of the Creative Commons Attribution (CC BY) license.

Keywords: groundwater-dependent ecosystems (GDEs); climate change impacts; groundwater recharge; sustainable water management; hydrological processes; Hailiutu River Basin

1. Introduction

Due to global warming, droughts are occurring more frequently, lasting longer, intensifying in severity, and expanding in spatial extent [1], exerting severe impacts on ecosystems in arid and semi-arid regions. As an essential part of the global ecosystem, ecosystems in semi-arid regions are highly sensitive to climate change and exhibit pronounced ecological fragility [2,3]. Semi-arid regions are characterized by acute water scarcity, and their ecological stability relies predominantly on the availability and distribution of water resources, particularly groundwater. Groundwater plays a pivotal role in semi-arid regions, serving as the principal source that sustains vegetation and maintains ecosystem stability during periods of low precipitation or drought. Natural vegetation primarily derives its water supply from three sources: precipitation, surface water, and groundwater. However, owing to low precipitation and high potential evaporation, surface water resources are severely limited, resulting in a notable increase in vegetation's dependence on groundwater [4–6]. Groundwater-dependent ecosystems (GDEs) are defined as ecosystems in which vegetation relies on groundwater to satisfy either a portion or the entirety of its water demand. In GDEs of arid regions, vegetation typically develops substantially greater belowground than aboveground biomass to adapt to environmental conditions and enhance water use efficiency [7,8].

Previous studies have shown that the afforestation programs piloted in China in 1999 and fully implemented nationwide starting in 2000, along with the steadily advancing desertification-control efforts since 2000, have significantly increased vegetation coverage in many regions [9]. This phenomenon is particularly pronounced in critical project areas, with the Hailiutu River Basin on the periphery of the Mu Us Sandy Land exhibiting a notable increase in vegetation cover. The Mu Us Sandy Land, a representative semi-arid region situated in the transitional zone between the Loess Plateau and arid areas, encompasses approximately 40,000 km^2 in north–central China and is predominantly influenced by the East Asian monsoon, with precipitation largely concentrated in the summer months [10,11]. Groundwater is crucial for sustaining local vegetation and managing regional water resources [12]. However, despite the significant decline in groundwater levels and the reduction in groundwater storage, the vegetation in this region has still become noticeably greener. An accelerated global water cycle may underlie this trend, as it elevates precipitation levels, consequently meeting the water needs of vegetation [13,14]; or from long-term adaptation of vegetation to arid conditions, with enhanced lateral roots and deeper rooting enabling access to deeper groundwater [15,16].

Ecological restoration has been identified as the dominant driver of the recent reversal of desertification in the Mu Us Sandy land, China, where large-scale afforestation and grassland rehabilitation projects have markedly improved vegetation cover and reduced land degradation [17]. However, in the Chinese Loess Plateau, revegetation efforts are approaching the sustainable limits of regional water resources, as the increased evapotranspiration associated with dense planting has placed substantial pressure on soil moisture and groundwater reserves [18]. These contrasting cases illustrate that while ecological restoration programs can achieve rapid improvements in vegetation conditions, they may simultaneously intensify water scarcity and exacerbate the vulnerability of groundwater-dependent ecosystems in arid and semi-arid regions.

https://doi.org/10.3390/land15010060

GDEs are affected by multiple factors, with climate factors being the primary driver of their dynamics. Previous studies across various regions in China and timescales indicate that vegetation indices are generally positively correlated with precipitation and temperature [19–21]. However, this response is not uniform globally and exhibits significant spatial heterogeneity. Global analyses show that in high-latitude and high-altitude regions of the Northern Hemisphere, growing-season normalized difference vegetation index (NDVI) is strongly positively correlated with temperature, indicating that temperature is the key limiting factor for vegetation growth [22,23]. In contrast, in arid regions characterized by limited precipitation, vegetation exhibits high sensitivity to rainfall variability due to prolonged water stress, rendering precipitation the primary controlling factor [24]. Piao et al. reported that at the national scale, rising temperatures are the primary driver of NDVI increases, whereas at regional scales, NDVI correlates more strongly with precipitation [25]. For groundwater-dependent vegetation, groundwater depth also significantly affects growth dynamics, with productivity decreasing as depth increases and stabilizing once a certain threshold is reached [26].

GDEs play a crucial role in arid regions, particularly in ecological fragile areas, forming a natural ecological barrier in the Mu Us Sandy Land and serving an irreplaceable function in stabilizing shifting sands, maintaining biodiversity, and ensuring regional ecological security [27]. GDEs and groundwater are closely interconnected and mutually regulated. In semi-arid regions, groundwater-dependent plants serve as sensitive indicators of groundwater fluctuations [28]. Under climate change, rising temperatures, altered precipitation patterns, and more frequent extreme events are profoundly affecting groundwater quantity and quality, potentially shifting GDEs from short-term water stress to long-term habitat degradation [29,30]. In addition, it can adversely affect their ecosystem services, including water quality regulation, climate regulation, and wind erosion control [31,32]. Understanding the interactions between GDEs, climate change, and groundwater variability provides critical scientific support for the sustainable use of water resources and the development of climate-adaptive ecological management strategies in ecologically fragile regions like the Mu Us Sandy Land.

In the context of climate change, understanding the interactions between GDEs and climatic drivers is essential for sustaining ecosystem stability and securing water resources. This study addresses the apparent paradox between vegetation greening and persistent groundwater depletion in GDEs, and evaluates the sustainability of their ecological functions. Using the Hailiutu River Basin, a typical ecologically vulnerable arid region, as a case study, we developed an integrated assessment framework to overcome limitations of previous research, including reliance on single data sources, insufficient cross-scale validation, and inadequate separation of climatic and groundwater influences. The framework integrates satellite-derived NDVI, groundwater storage anomalies (GWSAs), and field vegetation surveys, enabling validation across both regional and site scales. Trend analysis was applied to characterize two decades of change in vegetation cover and groundwater storage. A random forest model was used to analyze the relationships between various factors and NDVI and GWSA at the pixel scale, as well as the differences between GDE and non-GDE areas. Partial correlation analysis was then used to disentangle and quantify the independent effects of climate drivers (precipitation, temperature, and the standardized precipitation–evapotranspiration index (SPEI) and groundwater availability on vegetation growth, revealing their relative contributions. The SPEI, as an index representing moisture conditions across multiple time scales, is widely used in studies of arid regions [9,33,34]. Furthermore, by comparing the responses of GDEs and non-GDEs across spatial gradients, we identified distinct response mechanisms shaped by the interaction of climate forcing and groundwater constraints. The results emphasize the interactive impacts of climate

variability and groundwater depletion on vegetation dynamics, providing a robust quantitative basis for evaluating the vulnerability of GDEs and for developing targeted ecological restoration strategies in arid and semi-arid regions.

2. Materials and Methods

2.1. Study Area

The Hailiutu River Basin is located in the middle reaches of the Yellow River on the Ordos Plateau, within the transitional zone between the Loess Plateau and the Mu Us sandy land (Figure 1). The basin (108°38′–109°19′ E, 38°02′–38°51′ N) covers an area of approximately 2600 km^2, with elevations ranging from 1070 to 1442 m and the terrain generally high in the northwest and low in the south and central valley. The region has a semi-arid climate characterized by scarce and highly variable precipitation, with a long-term annual mean of about 350 mm. Approximately 70% of the annual precipitation occurs in summer and autumn, while strong potential evapotranspiration, averaging around 2100 mm per year, creates a pronounced water deficit [35].

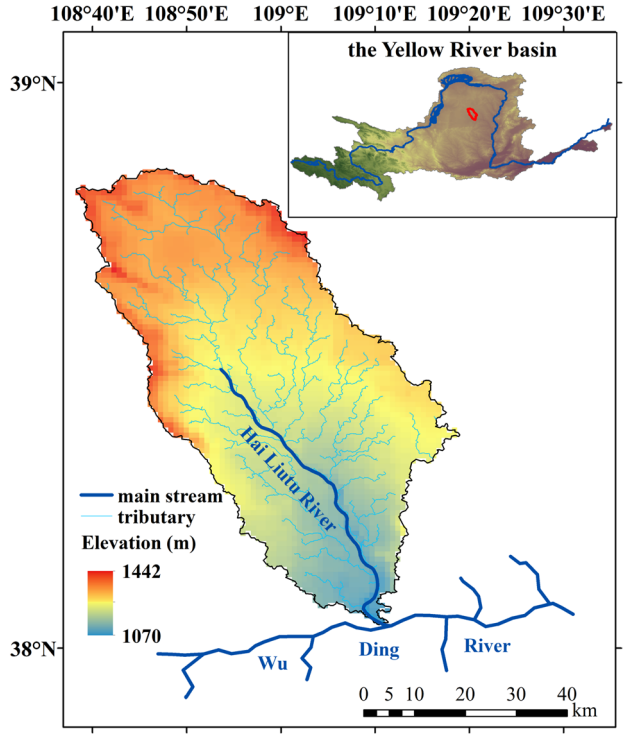

Figure 1. Study region of the Hailiutu River basin.

The Hailiutu River, a tributary of the Wuding River, has a length of about 85 km and a mean annual discharge of 8×10^7 m^3, Groundwater serves as the dominant source of streamflow and plays a critical role in sustaining local ecosystems due to the shallow groundwater table [35,36]. Vegetation in the basin is predominantly composed of xerophytic communities, including shrubs such as *Salix psammophila*, *Caragana korshinskii*, and *Artemisia ordosica*, as well as trees including *Salix matsudana* and *Populus simonii*. Herbaceous species are also widely distributed [37]. Both vegetation diversity and biomass are strongly influenced by groundwater availability, underscoring the intimate coupling between groundwater conditions and vegetation dynamics in semi-arid region [38,39]. In the context of extensive afforestation and vegetation restoration programs over the past two decades, human activities have intensified water extraction and land management interventions (covered 30% of the area), amplifying the uncertainty in groundwater-vegetation

balance and potentially altering the long-term sustainability of semi-arid ecosystems in the basin [36,40].

2.2. Field Survey of Vegetation in GDE

To further characterize the structure and ecological features of GDEs within the basin, a systematic field survey was conducted. In total, 28 vegetation sampling sites (GDEs: 12 plots; non-GDEs: 16 plots) were established to represent the major vegetation community types across different hydrological and geomorphological settings. Sampling locations were determined based on spatial vegetation patterns, practical accessibility, and their capacity to capture the representative characteristics of dominant habitat types. At each site, a standard quadrat survey method was employed to record vegetation characteristics. Depending on the vegetation type (Table 1), quadrat sizes were adjusted (e.g., 20 m × 20 m for tree layers, 5 m × 5 m for shrub layers, and 1 m × 1 m for herb layers). Within each quadrat, data were collected on species composition, canopy cover, plant height, plant density, and dominant species.

Table 1. Vegetation plot types surveyed in the study area.

Vegetation Type	Number
Tree	8
Shrub	12
Herb	8

The field survey provided a detailed dataset for assessing species diversity, community structure, and vegetation–groundwater relationships. These data were subsequently used to support the classification of vegetation communities associated with GDEs in the study area.

The GDE delineation is based on the integrated use of groundwater-depth data [35], field surveys of vegetation types, and remote sensing indicators of vegetation–groundwater. This study aims to evaluate groundwater dependence by constructing an index system composed of multiple environmental indicators, including groundwater depth, soil type, vegetation coverage, and evapotranspiration (Table S1). Each indicator reflects a different aspect of ecosystem dependence on groundwater and originates from different environmental layers such as surface, soil, and subsurface systems. Because these indicators influence groundwater dependence relatively independently, a weighted method is adopted to establish a comprehensive index and quantitatively evaluate the multi-factor groundwater dependence level.

2.3. Groundwater and Vegetation Changes

Normalized Difference Vegetation Index (NDVI) was calculated from surface reflectance as a normalized difference between the near-infrared (NIR) and red (RED) bands, defined as the difference between NIR and RED surface reflectance divided by their sum. This formulation captures the contrasting reflectance properties of healthy vegetation in these bands and provides a standardized measure of vegetation greenness. The NDVI data used in this study are derived from the monthly MODIS MOD13A3 product with a spatial resolution of 250 m, obtained from the NASA Earthdata platform. SPEI was calculated based on the climatic water balance derived from monthly precipitation and potential evapotranspiration, Potential evapotranspiration was estimated using the Penman-Monteith method, and the difference between precipitation and evapotranspiration was standardized to represent regional moisture conditions at different time scales.

Groundwater changes in this study are derived from the Gravity Recovery and Climate Experiment and its Follow-On mission (GRACE/GRACE-FO) groundwater storage anomaly (GWSA) dataset, which provides monthly estimates of regional-scale groundwater storage variations. All variables used in the analysis were resampled and unified to a spatial resolution of 0.01° to ensure consistency across datasets. To improve the spatial resolution of GWSA, a Machine Learning Downscaling Framework, integrating coarse-resolution observations from the GRACE/GRACE-FO with multi-source datasets, was developed to produce High-resolution Groundwater Storage Anomaly dataset (HWSA v1.0-GWSA) [41,42]. Based on the principle of water balance, TWSA can be decomposed into various components, including GWSA, soil moisture storage anomalies (SMSA), and others [43]. The dataset enhances spatial detail while preserving the physical consistency among hydrological components, providing an effective approach for monitoring fine-scale groundwater dynamics and regional water storage changes [44].

Groundwater data used in this study were derived from a combination of field-based monitoring and satellite-derived groundwater storage anomaly (GWSA) data. Field measurements include groundwater monitoring sites established in the Hailiutu River Basin in 2025 and long-term records from the National Monitoring Network Water Level Stations (2014–2024). Due to differences in observation scales between field-based and satellite-derived data, as well as the limited availability of continuous long-term monitoring, groundwater data from 2014 to 2025 (at a monthly scale) were selected for analysis. These data were used to validate GWSA trends and provide a reliable assessment of long-term regional groundwater variations (Figure S1 and Table S2).

3. Methods

The methodological innovation of this study lies in the cross-scale integration of long-term satellite observations, field-based monitoring data (groundwater storage anomaly and monitoring groundwater wells), and climatic variables (precipitation, temperature, and SPEI), enabling validation at both regional and site-specific scales. Trend analysis, Random Forest modeling, and partial correlation analysis were employed to quantify the spatiotemporal patterns of vegetation and groundwater changes, while disentangling the independent contributions of each driving factor to vegetation dynamics (calculated using R version 4.5.1). Furthermore, incorporating ecosystem vulnerability frameworks allows for a rigorous assessment of the sustainability and potential risks to groundwater-dependent ecosystems in arid regions. This integrated framework overcomes the limitations of previous studies, such as reliance on single data sources, insufficient cross-scale validation, and challenges in separating climate and groundwater effects, providing a comprehensive framework for analyzing ecohydrological interactions in dryland ecosystems.

3.1. Trend Analysis

The Theil-Sen slope method was used to determine the trends of climatic factors, groundwater and vegetation changes [45,46]. The Mann–Kendall (MK) test is a non-parametric statistical test for detecting trends and abrupt changes in time series [47–49]. The MK test is widely applied in hydrological analysis and climate change studies and is relatively robust against outliers. Therefore, this method was employed to calculate the linear slope of all indicators at the pixel scale and to test their significance. Trends were considered significant if the MK test yielded $p < 0.05$. The trend calculation formula is as follows:

$$Slope = Median\left(\frac{x_j - x_i}{t_j - t_i}\right), \forall j > \mathrm{i} \quad (1)$$

where x_i and x_j represent the i-th and j-th data points, respectively, and the slope > 0 indicates an increasing trend, whereas a slope value less than zero indicates a decreasing trend. The Mann–Kendall (MK) test statistic S is used to detect trends in a time series. S represents the sum of the signs of all pairwise differences between data points, indicating whether the overall trend is increasing, decreasing, or absent. The calculation formula is as follows:

$$S = \sum_{i=1}^{n-1} \sum_{j=i+1}^{n} \mathrm{sgn}(x_j - x_i),\ \mathrm{sgn} = (x_j - x_i) \begin{cases} +1,\ x_j - x_i > 0 \\ 0,\ x_j - x_i = 0 \\ -1, x_j - x_i < 0 \end{cases} \quad (2)$$

where n represents the total number of data points, and the variable x_i and x_j correspond to the i-th and j-th data points (j > i). The formulas for the standardized normal test Z_s and variance calculation are as follows:

$$Z_s = \begin{cases} \frac{S-1}{\sqrt{\mathrm{var}(S)}}, & S > 0 \\ 0, & S = 0 \\ \frac{S+1}{\sqrt{\mathrm{var}(S)}}, & S < 0 \end{cases}, \mathrm{var}(S) = \frac{n(n-1)(2n+5)}{18} \quad (3)$$

3.2. Partial Correlation Analysis

The dynamics of dryland vegetation are highly sensitive to climate change and mainly influenced by precipitation (Pre), temperature (Temp), and groundwater change (GWC). Therefore, partial correlation analysis was employed to examine the relationships between vegetation dynamics and different climatic factors, including Pre, Temp, GWC, and the SPEI. Regions where correlations reached statistical significance ($p < 0.05$) are shown in the Supplementary Figures S1–S7. The relative contributions and directional influences of the various factors were evaluated through comparison of their partial correlation coefficients.

3.3. Random Forest Analysis

In this study, a random forest regression model was applied to investigate the interactions between vegetation dynamics and groundwater (Figure 2). The model constructs an ensemble of decision trees through bootstrap aggregation (bagging), which enhances predictive stability and robustness. Owing to its capacity to capture nonlinear relationships and handle heterogeneous data, the random forest method has been widely employed in tasks such as variable importance evaluation and key driver identification [50,51]. The algorithm relies on out-of-bag (OOB) samples—observations excluded from the training of individual trees—to estimate model error and variable relevance. By introducing random noise into a predictor X and comparing the resulting OOB prediction error with the error before adding the noise, the model quantifies the contribution of that variable: a larger increase in OOB error implies greater importance [52]. This approach not only avoids the adverse effects of multicollinearity among features on model accuracy, but also provides an unbiased performance evaluation metric comparable to K-fold cross-validation [53,54]. A smaller OOB error and an R^2 value closer to 1 indicate better model performance [55]. After comparison, the hyperparameters of the random forest model were set as follows: the number of estimators was 100 and the minimum sample leaf was 5, while no restriction was imposed on the maximum depth. The complete process of the random forest regression model is detailed in Figure 2.

In this study, we quantified the multi-ecohydrological interactions between groundwater and vegetation in GDEs using a cross-validation framework that combines random forest contribution analysis with partial correlation analysis. Specifically, the random forest model used GWSA as the dependent variable, with Pre, Temp, SPEI and NDVI as the

independent variables. Conversely, the effects of groundwater and climate on vegetation productivity were evaluated using NDVI as the dependent variable. To address multicollinearity among predictors, variance partitioning and permutation-based importance measures were applied, ensuring robust estimation of individual factor contributions. The regression estimates based on partial correlation analysis were further validated using a random forest model, which accounts for the interactive effects between climatic and hydrological factors and provides spatially explicit quantification of their relative importance across GDEs and non-GDEs.

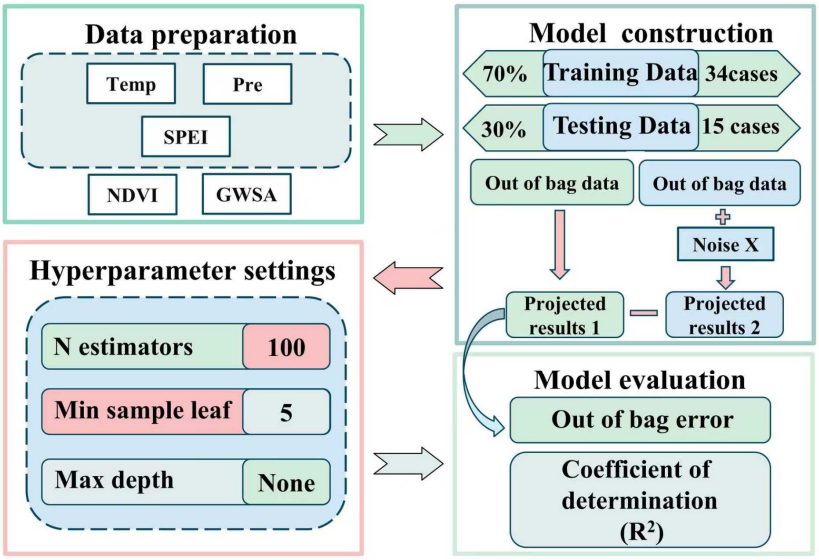

Figure 2. Logical framework for Random Forest (RF) model training and validation. The random forest model in this study consists of four main components: data preparation, model construction, hyperparameter settings, and model evaluation. Among them, the Out-of-Bag error (OOBError) is not only an indicator for assessing the relative importance of variables but also an important criterion for evaluating model performance.

4. Result

4.1. Spatiotemporal Changes in Meteorological and Hydrological Variables

Spatiotemporal variations in meteorological conditions, groundwater storage, drought, and vegetation dynamics during the growing season (April–October) in the Hailiutu River Basin were assessed by calculating Theil–Sen slope trends for each variable from 2002 to 2022 (Figure 3). The analysis indicates a basin-wide increase in precipitation, an overall enhancement of vegetation activity ($p < 0.005$, covered by 95% area in Figure S3), and a persistent decline in groundwater storage anomaly (GWSA, $p < 0.005$ in the whole region). Moreover, the positive SPEI (not significant) trend indicated a slight increase in regional moisture availability during the study period. Regional mean Theil–Sen slope values provide quantitative evidence of the basin-scale trends. Precipitation exhibited a significant increasing trend (0.0735 mm/yr), while temperature remained essentially stable, showing only a slight change (−0.0006 °C/yr). The SPEI increased at a rate of 0.0207/yr, suggesting enhanced regional water availability during the study period. Similarly, vegetation activity demonstrated a modest but consistent positive trend (0.0049/yr). In contrast, the GWSA revealed a markedly negative slope (−11.19 mm/yr), reflecting simultaneous enhancement of moisture availability and vegetation productivity alongside persistent depletion of groundwater resources across the Hailiutu River Basin.

In addition, regional mean Theil–Sen slope values highlight distinct differences between non-GDE and GDEs areas (Figure 4). Precipitation, temperature, and SPEI increased in both regions, with non-GDEs showing higher rates of change in precipitation

(0.742/yr in non-GDEs and 0.719/yr in GDEs), temperature (−0.001 °C/yr in non-GDEs and 0.0004 °C/yr in GDEs), and SPEI (0.0212/yr in non-GDEs and 0.0195/yr in GDEs), while NDVI increased slightly more in GDEs (0.0048/yr in non-GDEs and 0.0052/yr in GDEs), indicating that meteorological and ecological variables exhibited spatial variation in their trends. In contrast, the GWSA declined significantly in both non-GDEs and GDEs (−11.20/yr and −11.18/yr, respectively), demonstrating persistent basin-wide groundwater depletion. Overall, while precipitation, water availability, and vegetation activity improved across the basin, the pronounced decline in groundwater storage highlights an increased imbalance between water supply and ecological demand across the basin.

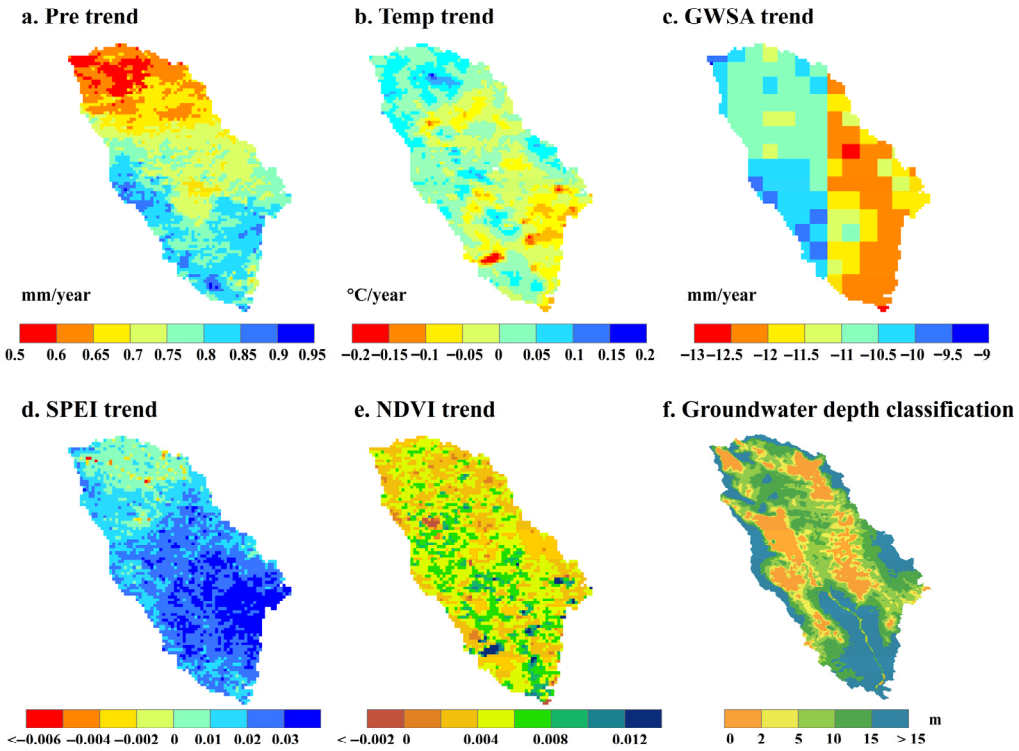

Figure 3. Spatial and temporal trends of meteorological, hydrological, and ecological variables in the Hailiutu River Basin. (**a**–**e**) The trend of precipitation, temperature, SPEI, NDVI, and groundwater storage anomaly, (**f**) Groundwater table depth classes as an indicator of groundwater conditions. (**f**) is modified from Dong et al., 2024 [35].

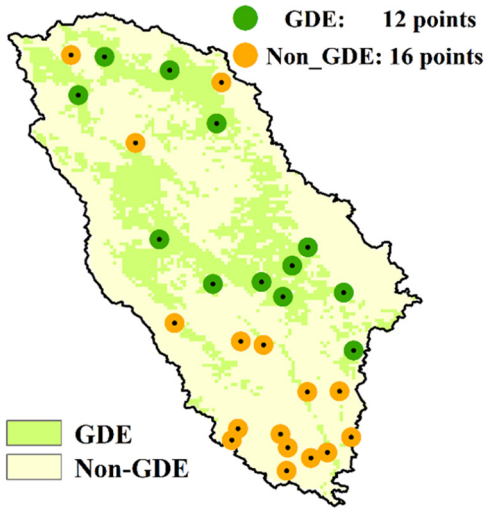

Figure 4. Spatial distribution of GDE and non-GDE areas, along with vegetation sampling sites.

To further characterize the GDEs within the basin, a total of 28 vegetation sampling sites were surveyed across representative vegetation community types (Figure 4). The survey documented species composition, canopy cover, plant height, density, and dominant species, enabling the classification of vegetation layers into trees, shrubs, and herbs. Typical species recorded included *Populus angustifolia*, *Pinus sylvestris* var. *mongolica*, *Salix psammophila*, *Artemisia ordosica*, and *Achnatherum splendens*, reflecting the structural and compositional features of groundwater-dependent vegetation communities in the Hailiutu River Basin.

4.2. Temporal Changes in Groundwater and Vegetation of GDE and Non-GDE Area

Groundwater storage decreased while vegetation greenness increased in both GDE and non-GDE areas from 2002 to 2022 year (Figure 5). In the Hailiutu River Basin, groundwater storage anomalies (GWSAs) showed a significant declining trend of –11.406 mm/yr in GDE and −11.397 mm/yr in non-GDE areas (R^2 = 0.92, $p < 0.01$), whereas NDVI exhibited a significant increase, with rates of 0.005/yr in GDE areas (R^2 = 0.88, $p < 0.01$) and 0.004/yr in non-GDE areas (R^2 = 0.91, $p < 0.01$). These results indicate that despite the continuous depletion of groundwater resources, vegetation conditions improved in both GDE and non-GDE areas, with GDE areas showing slightly higher NDVI growth than non-GDE areas, suggesting a relative advantage in vegetation recovery.

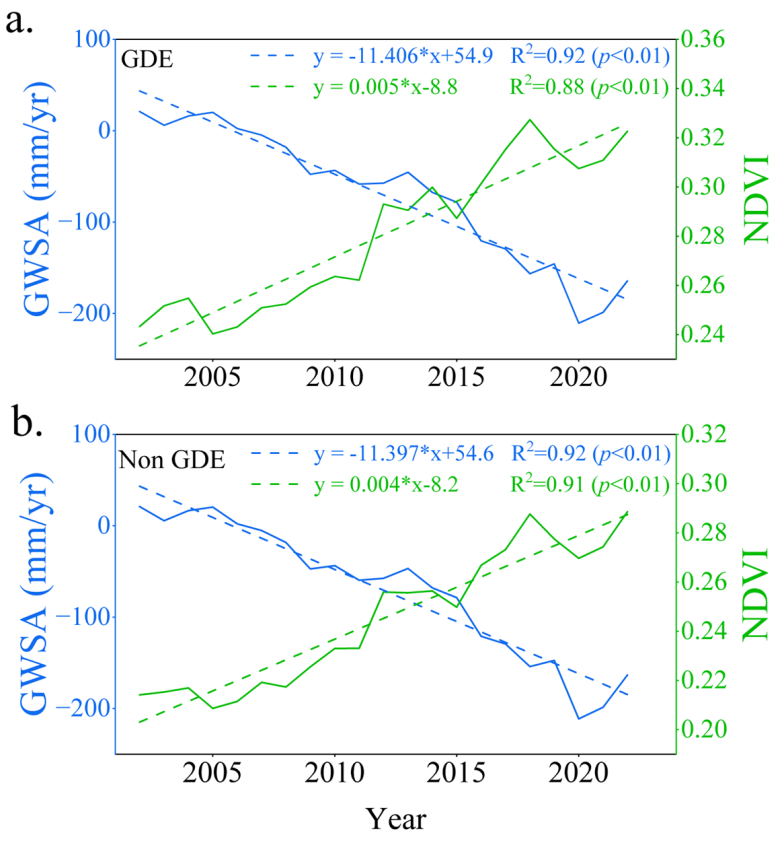

Figure 5. Groundwater storage anomalies and vegetation changes in GDE and non-GDE areas. (**a**) GWSA and NDVI in GDE areas, (**b**) GWSA and NDVI in non-GDE areas.

The groundwater table depth and terrestrial water storage in the Hailiutu River Basin indicate a sustained decline in groundwater at the regional scale, highlighting ongoing depletion of subsurface water resources (Table S2). An increasing trend in groundwater table depth was observed in GDE, non-GDE, and the overall study area, reflecting a progressive decline in groundwater levels (Figure 6). In GDE areas, the increase in groundwater table

depth was relatively gradual (0.0008 m/yr, $p < 0.05$), whereas in non-GDE areas the increase was more pronounced (0.002 m/yr, $p < 0.05$), demonstrating that groundwater depletion is pervasive across both ecosystem types and continues to progress over time.

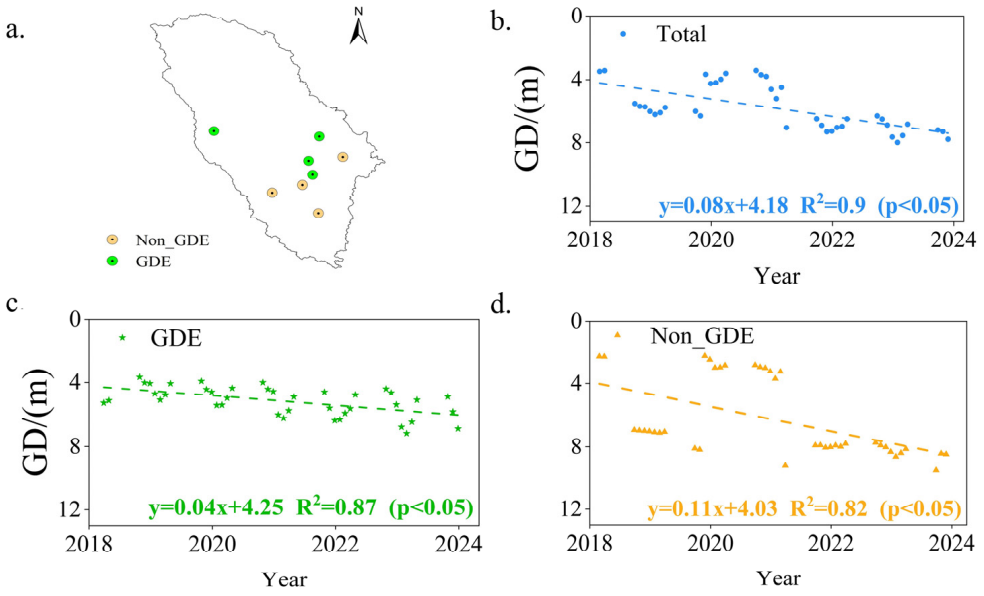

Figure 6. Groundwater depth (GD) changes at national monitoring stations in the Hailiutu River Basin in GDE and non-GDE areas. (**a**) Distribution of national monitoring stations, (**b**) GD changes in total stations, (**c**) GD changes in stations in GDE areas, (**d**) GD changes in stations in non-GDE areas. The dashed line represents the regression line of GD.

4.3. Drivers of Vegetation and Groundwater Variations: A Cross-Validation Analysis Using Partial Correlation and Random Forest Models

For vegetation variations (NDVI), both partial correlation analysis and the random forest model consistently show that groundwater availability (GWSA) is the dominant driver (Figures 7 and 8). In the partial correlation results, the correlation coefficients between NDVI and groundwater are −0.785 in GDE areas and −0.782 in non-GDE areas, with an overall value of −0.783. This strong negative relationship indicates that vegetation growth is highly sensitive to groundwater changes, particularly in groundwater-dependent ecosystems, reflecting intense ecohydrological interactions. The random forest analysis further reinforces these findings, showing even higher contribution values of 0.873 for GDE regions and 0.872 for non-GDE regions.

For groundwater variations (GWSA), both partial correlation analysis and the random forest model consistently identify vegetation dynamics (NDVI) as the most influential factor (Figures 9 and 10). In the partial correlation analysis, NDVI shows strong negative correlations with groundwater anomalies, with coefficients of −0.785 in GDE areas,−0.782 in non-GDE areas, and −0.783 overall, indicating that increases in vegetation activity are closely associated with reductions in groundwater storage. This relationship is especially pronounced in groundwater-dependent ecosystems, highlighting significant ecohydrological coupling. The random forest analysis further confirms the dominant role of NDVI, with contribution values of 0.857 overall, 0.856 in GDE regions, and 0.856 in non-GDE regions. These consistently high values underscore that vegetation growth is the primary driver of groundwater variability.

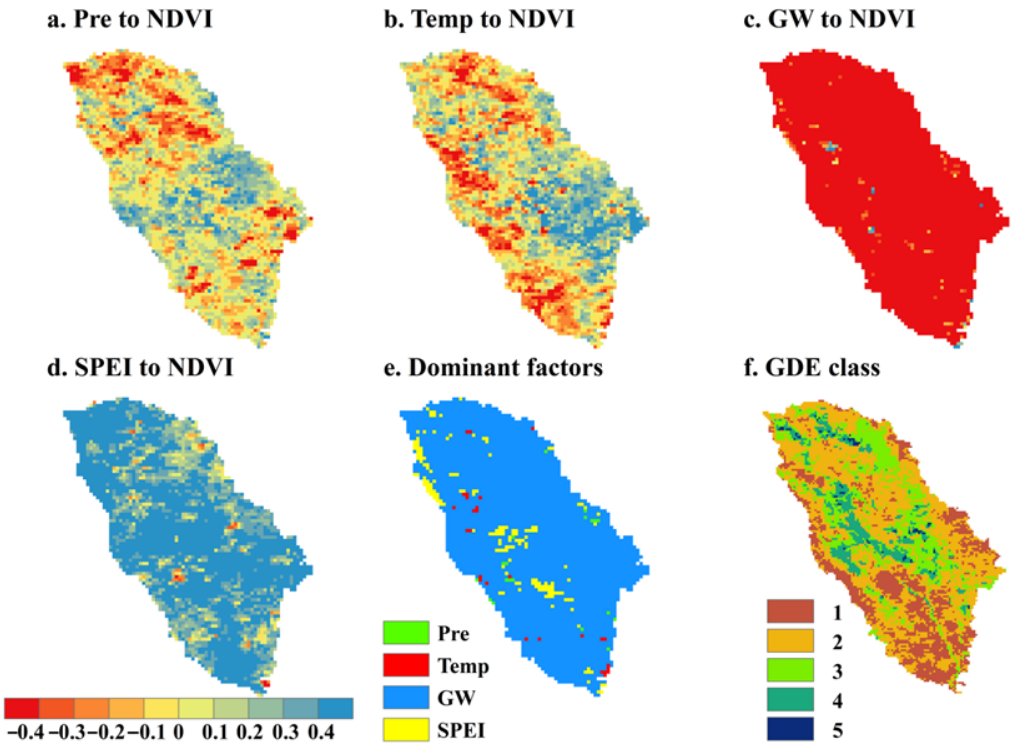

Figure 7. Correlation of meteorological and hydrological changes to vegetation based on partial correlation analysis. (**a**–**d**) Contribution of precipitation, temperature, SPEI, and groundwater storage anomaly to NDVI changes. (**e**) Dominant factors. (**f**) Depth to groundwater and groundwater dependence levels (Level 1 to 5, with a higher score indicating a greater degree of dependency) of vegetation in the Hailiutu River Basin. (**f**) is modified from Dong et al., 2024 [35].

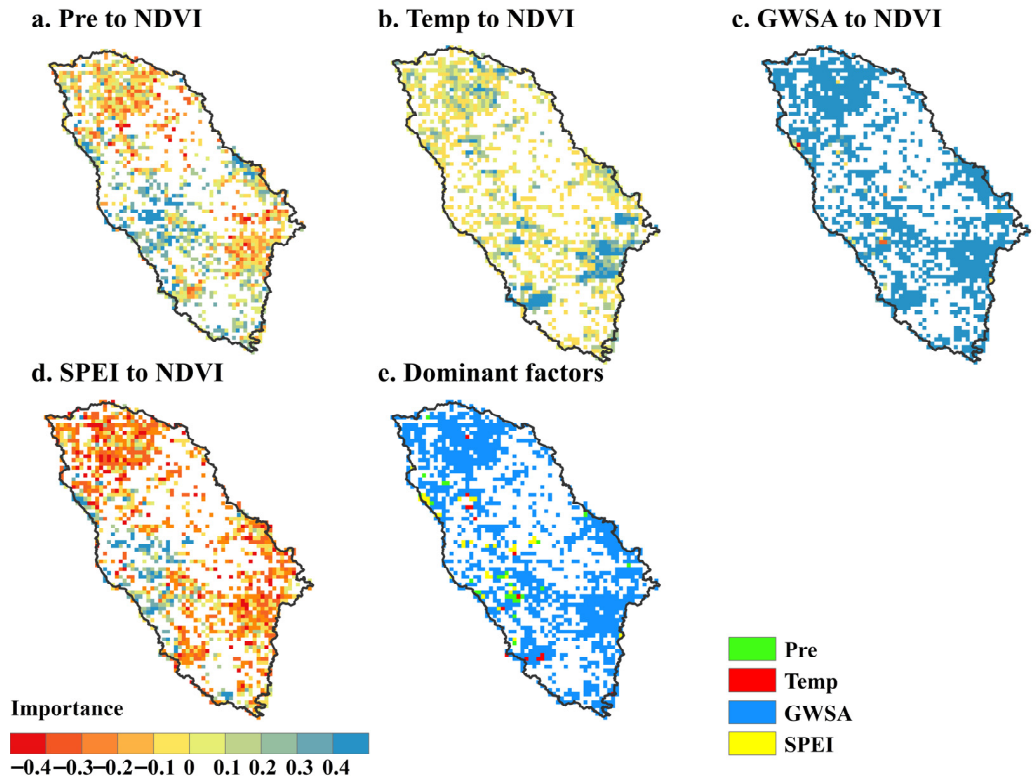

Figure 8. Contribution of meteorological and hydrological changes to vegetation based on Random Forest analysis. (**a**–**d**) Contribution of precipitation, temperature, SPEI, and groundwater storage anomaly to NDVI changes. (**e**) Dominant factors.

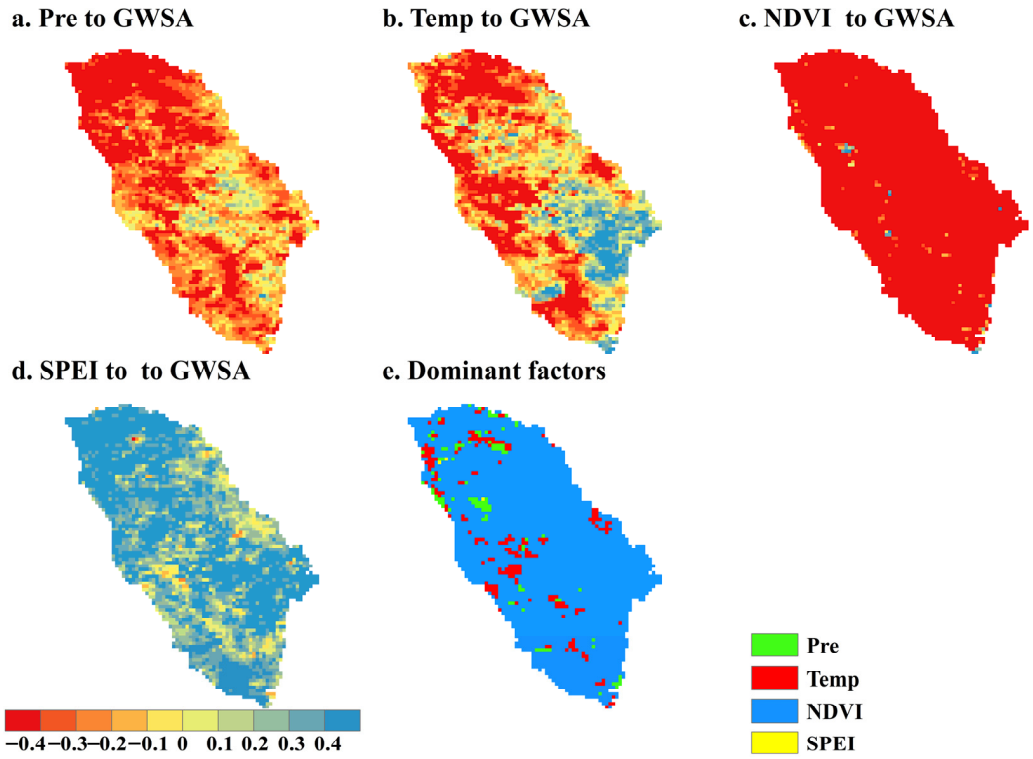

Figure 9. Contribution of meteorological factors and vegetation changes to groundwater based on partial correlation analysis. (**a**–**d**) Contribution of precipitation, temperature, NDVI and SPEI to groundwater storage anomaly (GWSA) changes. (**e**) Dominant factors.

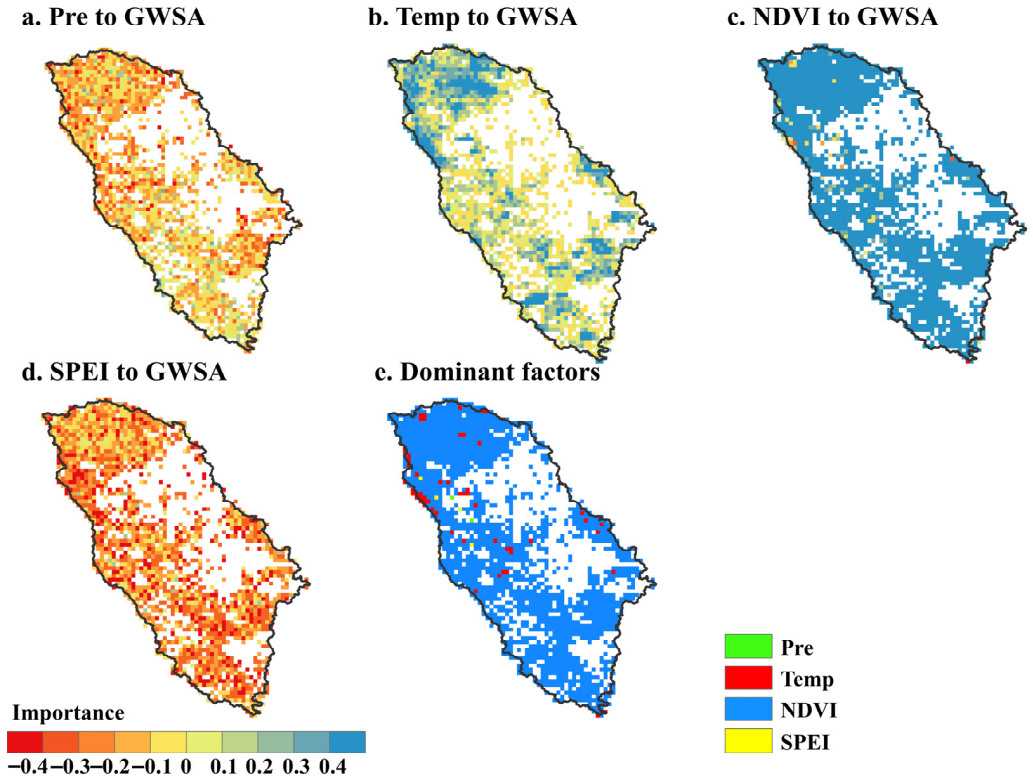

Figure 10. Contribution of meteorological factors and vegetation changes to groundwater. based on Random Forest analysis. (**a**–**d**) Contribution of precipitation, temperature, NDVI and SPEI to groundwater storage anomaly (GWSA) changes. (**e**) Dominant factors.

4.3.1. Vegetation Responses to Climate and Groundwater Storage Changes in GDE and Non-GDE

Precipitation and temperature exhibit comparatively smaller contributions. In partial correlation analysis, their contributions range from 0.003 to 0.017 for precipitation and 0.017 to 0.023 for temperature (Figure 7). In the random forest model, their contributions increase to 0.139–0.140 for precipitation and 0.174–0.175 for temperature, confirming that climate factors have a comparatively weaker contribution (Figure 8). SPEI shows the smallest contributions, ranging from 0.014 to 0.015 in the random forest model and 0.424–0.453 in partial correlation analysis. Overall, the consistent results of both methods validate each other, groundwater availability is the dominant control on vegetation variation, particularly in groundwater-dependent ecosystems, while climate factors have a relatively minor role. In the Hailiutu River Basin, precipitation contributed positively to vegetation dynamics in the central region, whereas temperature exerted a positive influence in the eastern region.

Groundwater, however, exhibited a negative contribution to vegetation growth. In the whole region, the contributions of climatic and hydrological factors to vegetation dynamics varied spatially, and the significance of partial correlations for all factors can be seen in Figure S4. Precipitation contributed positively to vegetation growth, particularly in the central region, with a contribution value of 0.0171/yr in non-GDEs and 0.0032/yr in GDEs, while temperature exerted a positive influence mainly in the eastern region, with contributions of 0.0168/yr in non-GDEs and 0.0227/yr in GDEs. In contrast, GWSA had a negative effect on vegetation growth, with contribution values of −0.7824/yr in non-GDEs and −0.7854/yr in GDEs, indicating a consistent negative impact across ecosystems. NDVI trends were positively influenced by SPEI, with respective contributions of 0.4237/yr in non-GDEs and 0.4533/yr in GDEs, highlighting the critical role of regional water availability in sustaining vegetation dynamics.

4.3.2. Groundwater Responses to Climate and NDVI Changes in GDE and Non-GDE

Both the partial correlation analysis and the random forest model consistently show that NDVI exerts the strongest negative effect on groundwater anomalies, indicating that vegetation variation plays a dominant role in groundwater dynamics (Figures 9 and 10). SPEI presents a positive contribution, reflecting that wetter conditions are associated with higher groundwater levels. The contributions of precipitation and temperature are relatively smaller but show consistent trends across GDE and non-GDE regions. In the Hailiutu River Basin, vegetation exerted the strongest negative influence on groundwater variations, with consistently negative contributions across the basin (Figures 9 and S5). NDVI showed contribution values of −0.7824/yr in non-GDEs and −0.7854/yr in GDEs, indicating that vegetation water consumption plays a dominant role in groundwater decline. Climatic drivers exhibited weaker but spatially heterogeneous effects. Precipitation contributed negatively to groundwater, with values of −0.2924/yr in non-GDEs and −0.3097/yr in GDEs, suggesting that contribution of precipitation recharge was limited in this basin. Temperature also showed a negative contribution of −0.1520/yr in non-GDEs and −0.1752/yr in GDEs, reflecting enhanced evapotranspiration under warming conditions. By contrast, SPEI contributed positively to groundwater dynamics, with values of 0.3685/yr in non-GDEs and 0.3879/yr in GDEs, highlighting the role of drought alleviation and climatic wetness in maintaining groundwater stability. Overall, vegetation consumption dominated groundwater variations, while climatic factors, particularly drought conditions, exerted regionally significant influences.

The results reveal significant multi-ecohydrological interactions between groundwater and vegetation in the Hailiutu River Basin (Figures 9 and 10). Groundwater storage anomalies (GWSAs) exhibited a consistently negative contribution to vegetation dynamics, with

correlation coefficients of −0.7824 in non-GDE areas and −0.7854 in GDE areas, indicating that groundwater depletion imposes strong constraints on vegetation growth across GDEs. In contrast, vegetation dynamics, represented by NDVI, contributed negatively to groundwater change, with correlation coefficients of −0.2975 across the entire basin, highlighting the role of vegetation water consumption in driving groundwater decline. Climatic factors further modulated these interactions, precipitation positively influenced vegetation growth (contributions of 0.0171/yr in non-GDEs and 0.0032/yr in GDEs), whereas temperature showed positive effects in the basin (0.0168/yr in non-GDEs and 0.0227/yr in GDEs). SPEI also positively affected vegetation (0.4237/yr in non-GDEs and 0.4533/yr in GDEs), reflecting the importance of water availability. These findings demonstrate that vegetation consumption exerts the dominant influence on groundwater variations, while groundwater simultaneously constrains vegetation growth, particularly in areas where declining GWSA coincides with reduced NDVI. Climatic factors, especially precipitation and drought conditions, further modulate the magnitude and spatial heterogeneity of these interactions, highlighting an asymmetric ecohydrological feedback system in the Hailiutu River Basin.

4.4. Model Validation and Uncertainty Analysis

To evaluate the reliability of the machine learning models, this study conducted an integrated assessment of model accuracy and sources of uncertainty. For accuracy validation, five-fold cross-validation was employed to reduce random errors arising from data partitioning, and metrics such as the coefficient of determination (R^2) and OOB error were used to assess model fitting and predictive performance. Results show that pixel-scale R^2 values are concentrated around 0.7, while OOB errors are largely near 0.01 (Figures S6 and S7), indicating strong generalization capability without evident overfitting or underfitting.

For uncertainty analysis, we examined contributions from data, model parameters, and factor selection. First, uncertainties in the input data mainly stem from spatiotemporal heterogeneity and remote sensing measurement errors, which directly affect the reliability of the model outputs. NDVI and groundwater storage, as the most influential variables, also introduced the largest uncertainties. Second, the sensitivity analysis revealed that changes in parameters, such as tree depth and learning rate, can cause minor fluctuations in the model performance. Additionally, intense human activity in the study area may lead to an overestimation of the effects of rainfall, temperature, and other environmental factors. Overall, the constructed machine learning models exhibited high accuracy and stability; however, their uncertainties were still primarily driven by spatiotemporal variability in the data and were influenced to some extent by parameterization and factor selection. As random forest and partial correlation models are statistical in nature, they capture only correlations rather than causal mechanisms; therefore, future work may integrate physical process-based models to further investigate causal relationships.

5. Discussion

The analysis of Theil–Sen slopes and contribution values indicates that vegetation dynamics in the Hailiutu River Basin are driven by a combination of climatic, hydrological, and anthropogenic factors, with spatial heterogeneity across GDEs and non-GDE areas. NDVI trends were consistently positively affected by precipitation, particularly in the central region, emphasizing the critical role of water supply in driving vegetation growth within this semi-arid basin (Table 2) [56,57]. Temperature exerted a positive effect mainly in the eastern region, suggesting that moderate warming during the growing season may prolong the growing period or enhance photosynthetic activity in specific areas [58,59]. The SPEI, which represents regional water availability, showed the largest positive contribution

to NDVI trends across both GDEs and non-GDEs, highlighting that vegetation responds strongly to interannual variations in moisture balance [60,61]. Non-GDE areas displayed slightly higher contributions from precipitation and SPEI compared to GDEs, whereas NDVI increases were slightly greater in GDEs, suggesting that groundwater-dependent ecosystems may exhibit higher vegetation sensitivity even when meteorological conditions are moderate [6]. These results indicate that climatic factors, particularly precipitation combined with drought indices indicating a warming and wetting trend, provide the necessary water resources for vegetation growth [62–64]. Since 2000, afforestation and other land management programs have partially mitigated ecological stress, emphasizing that anthropogenic activities can reinforce or offset natural trends, particularly in areas with limited water availability [65–67]. Therefore, the observed improvements in NDVI over the past two decades reflect the combined effects of climatic conditions and ecological restoration measures. In addition to these natural drivers, human activities emerged as a key determinant of vegetation cover change. Since 2000, extensive afforestation programs have partially mitigated ecological stress, underscoring the predominant role of anthropogenic factors in regulating vegetation dynamics across the basin. Overall, while precipitation, temperature, and water availability promoted vegetation growth, the negative influence of groundwater depletion underscores the complex interactions between natural and human drivers in shaping vegetation trends.

Table 2. Species composition of tree, shrub, and herb layers in the Hailiutu River Basin.

Vegetation	Common Species	Scientific Name
Tree	Drought Willow, Black Poplar, Korean Pine	*Populus angustifolia*, *Populus nigra*, *Pinus sylvestris* var. *mongolica*
Shrub	Sand Willow, Sand Sagebrush, Nitraria, Calligonum, Small-leaved Caragana, Sabina, Altai Arctic Daisy, Gobi Onion, Sand Blue Thistle	*Salix psammophila*, *Artemisia ordosica*, *Nitraria tangutorum*, *Calligonum mongolicum*, *Caragana microphylla*, *Sabina przewalskii*, *Cremanthodium arcticum*, *Allium gobicum*, *Echinops setifer*
Grassland	Feather Grass, Sand Wormwood, Suaeda, *Suaeda physophora*, Alfalfa	*Achnatherum splendens*, *Artemisia scoparia*, *Suaeda glauca*, *Suaeda physophora*, *Medicago sativa*

GWSA has exhibited a markedly negative trend across the basin, with similar declines in both GDEs and non-GDEs, indicating a persistent depletion of subsurface water resources [68–70]. The negative contribution of groundwater to vegetation growth suggests that reductions in groundwater availability may limit root-zone water supply (see Table S2), particularly during dry periods or in deep-rooted plant communities [39,71,72]. In GDEs, where vegetation relies directly on shallow groundwater, the depletion may reduce ecosystem resilience and constrain further increases in NDVI, even under favorable precipitation and temperature conditions [73,74]. In non-GDE areas, although vegetation depends primarily on precipitation and surface water, the regional decline in groundwater can indirectly influence surface water availability and soil moisture retention, thereby moderating vegetation growth [75,76]. These findings underscore the complex interactions between surface climate variables, groundwater resources, and vegetation dynamics. While precipitation, temperature, and SPEI promote vegetation growth, the continued depletion of groundwater represents a limiting factor that may constrain long-term ecosystem productivity and the sustainability of afforestation programs [77–80]. Consequently, future vegetation management in the Hailiutu River Basin should incorporate groundwater conservation measures in conjunction with ecological restoration efforts to ensure a balanced water supply and sustain ecosystem functioning under changing climatic conditions.

Long-term and intensive groundwater abstraction for irrigation and ecological restoration has continuously exceeded the natural recharge capacity [36,40]. In semi-arid regions, only a small fraction of precipitation contributes to effective deep groundwater recharge, as most rainfall is lost through evapotranspiration and surface runoff. Moreover, the observed vegetation greening further enhances transpiration, which reduces the amount of water available for groundwater replenishment. These combined factors help explain why groundwater storage in the Hailiutu River Basin continues to decline despite increased surface moisture availability [26,38,40]. In many typical arid and semi-arid regions, vegetation conditions have shown significant improvement in recent decades, largely driven by large-scale ecological restoration programs and afforestation efforts [81,82]. However, the greening trend has often coincided with a continuous decline in groundwater levels.

Large-scale ecological restoration projects have been implemented, particularly in regions such as the Mu Us Sandy Land and the Loess Plateau. While these efforts can rapidly improve vegetation conditions, they may simultaneously exacerbate water scarcity in arid and semi-arid areas and increase the vulnerability of groundwater-dependent ecosystems [18,83]. Due to the buffering capacity of groundwater, the ecological groundwater table threshold should be understood as a conditional threshold that varies with vegetation type, water source composition, and climatic context. Under conditions where multiple water sources are available, the manifestation of groundwater thresholds may be obscured by compensatory contributions from precipitation and soil moisture [28,84]. In the Hailiutu River Basin, however, groundwater levels have shown a persistent decline, indicating that the buffering capacity is gradually being lost and that vegetation may become increasingly vulnerable once critical thresholds are exceeded [36]. Under the growing uncertainty associated with future climate change, the management of vegetation–groundwater interactions in this basin requires adaptive measures such as optimizing species selection and planting density, improving water-use efficiency, and integrating groundwater monitoring into ecosystem management. Implementing these strategies is essential to reconcile ecological resilience with the sustainable management of groundwater resources.

Future climate change and anthropogenic activities are likely to further modulate groundwater–vegetation interactions in the Hailiutu River Basin. Climate projections and regional hydrological modeling suggest that increasing temperatures, shifts in precipitation regimes, and heightened drought frequency may alter both surface and subsurface water availability, thereby affecting vegetation dynamics. Extreme climate events, including wildfires, floods, and droughts, have become increasingly frequent. Climate change has transformed droughts from slowly developing processes into rapid and intensified episodic events, particularly affecting ecosystem productivity [6,85,86]. Water resources are scarce in many regions of the world, with northwestern India being a typical example. Satellite-based estimates of groundwater depletion indicate that groundwater in this region is being extracted faster than it is naturally replenished, primarily due to irrigation and other anthropogenic activities. Prolonged groundwater depletion increases the vulnerability of ecosystems, potentially affecting physiological functions and community structure, and heightening the risk of exceeding critical hydrological thresholds [85,87]. Previous studies have shown that ecosystems have limited resilience to such abrupt droughts. Between 2001 and 2022, vegetation in hotspots (including East Asia, western North America, and Northern Europe) experienced up to a 27% decline in resistance to sudden droughts, primarily due to increases in vapor pressure deficit, higher temperatures, and heightened sensitivity of vegetation structure to water availability. In arid regions, groundwater availability is a crucial hydrological foundation for maintaining terrestrial ecosystem stability and plays a central role in regulating plant water-use strategies and sustaining ecological functions [6,86,88]. Under drought stress, groundwater serves as a deep and relatively

stable water source, supporting plant physiological functions and maintaining the balance of ecosystem water cycles. Moreover, groundwater-dependent vegetation undergoes successional changes under long-term groundwater extraction. In the California, nearly 20 years of groundwater depletion shifted dominant groundwater-dependent vegetation from herbaceous plants to shrubs, and water-source dependence transitioned from groundwater to precipitation [89,90]. Approximately 83% of this change can be explained by groundwater table fluctuations, highlighting groundwater dynamics as a key driver of vegetation community structure and coverage [28,89].

6. Conclusions

GDEs cover 30% of the Hailiutu River Basin, constituting a critical component of regional ecological stability. In this study, we systematically evaluated vegetation responses to climate variability and groundwater depletion using remote sensing NDVI data, GWSA records, and field vegetation surveys, accounting for both regional and plot-scale influences. Trend analysis and partial correlation analysis were used to construct a quantitative framework for assessing the relative contributions of climate and groundwater to vegetation dynamics, and to compare the spatial differences in their contributions between GDEs and non-GDEs. Over the past two decades, remote sensing data of GWSA and NDVI revealed a continuous decline in groundwater storage accompanied by significant vegetation greening, especially in GDEs. Groundwater monitoring data from observation wells together with vegetation plot surveys confirmed the depletion consistently suggest a strong reciprocal coupling between vegetation and groundwater. Vegetation dynamics are primarily driven by groundwater availability, especially in groundwater-dependent ecosystems. Conversely, groundwater variations are most strongly influenced by vegetation. This consistency across methods confirms that ecohydrological interactions are the key driver of both vegetation and groundwater changes. These findings demonstrate that, while climate variability supports vegetation recovery, the continued decline in groundwater storage is likely to continue intensifying water scarcity and increasing the vulnerability of GDEs in arid and semi-arid regions.

Supplementary Materials: The following supporting information can be downloaded at: https://www.mdpi.com/article/10.3390/land15010060/s1.

Author Contributions: L.Z.: Data collection, Methodology, Validation, Writing—Original Draft, Funding Acquisition. L.X.: Methodology, Validation, Writing—Original Draft. B.S.: Methodology, Formal Analysis, Writing—Original Draft. P.W.: Conceptualization, Writing—Review and Editing. T.W.: Conceptualization, Writing—Review and Editing. G.Q.: Writing—Review and Editing. H.W.: Data collection, Writing—Review and Editing. X.J.: Writing—Review and Editing. All authors have read and agreed to the published version of the manuscript.

Funding: This work was supported by the Geological Survey Project of the China Geological Survey (DD202307005), National Natural Science Foundation of China (No. 41877199), Key Research and Development Program of Shaanxi Province (2021ZDLSF05-01), Sanqin Talents Special Support Program "Study on the Interaction Between Water and Ecology in the Southeastern Edge of the Mu Us Sandy Land", Study on the Relationship between Joint Structure and Soil Erosion Causation Mechanism in the Husi Gully Watershed, the Pisha Sandstone Distribution Area of the Middle Reaches of the Yellow River (2024JC-YBMS-240).

Data Availability Statement: Monthly precipitation data at 1 km spatial resolution for China are available from https://doi.org/10.5281/zenodo.3114194. Land Surface Temperature (LST) at 1 km spatial resolution derived from MODIS/LST061/MYD11A1 is accessible through https://lpdaac.usgs.gov/products/myd11a1v006/ (accessed on 13 March 2025). The drought index of SPEI dataset at 1 km spatial resolution across Chinese Mainland is sourced from https://www.scidb.cn/en/

detail?dataSetId=968592537239420928#p2 (accessed on 18 March 2025). Normalized Difference Vegetation Index at 1 km spatial resolution (MODIS/061/MOD13C2) is obtained from https://lpdaac.usgs.gov/products/mod13c2v061/ (accessed on 20 March 2025). Groundwater Storage Anomaly (HWSA v1.0-GWSA) data based on GRACE/GRACE-FO are available at https://data.tpdc.ac.cn/en/data/42176bad-0d38-4a84-9f87-3c2c06eb19b8 (accessed on 1 April 2025), with a spatial resolution of 0.05° at monthly scale. Elevation data is available at https://www.tpdc.ac.cn/zh-hans/data/12e91073-0181-44bf-8308-c50e5bd9a734/ (accessed on 8 April 2025). The depth to groundwater and the groundwater dependence levels of vegetation in Hailiutu River Basin were obtained from https://doi.org/10.12029/gc20220526002.

Acknowledgments: The authors are grateful to the editors and anonymous reviewers for their constructive comments.

Conflicts of Interest: The authors declare no conflicts of interest.

References

1. Li, Q.; Ye, A.; Wada, Y.; Zhang, Y.; Zhou, J. Climate change leads to an expansion of global drought-sensitive area. *J. Hydrol.* **2024**, *632*, 130874. [CrossRef]
2. Wang, Z.; Li, X.; Mao, Y.; Li, L.; Wang, X.; Lin, Q. Dynamic simulation of land use change and assessment of carbon storage based on climate change scenarios at the city level: A case study of Bortala, China. *Ecol. Indic.* **2022**, *134*, 108499. [CrossRef]
3. Zhuang, Q.; Shao, Z.; Huang, X.; Zhang, Y.; Wu, W.; Feng, X.; Lv, X.; Ding, Q.; Cai, B.; Altan, O. Evolution of soil salinization under the background of landscape patterns in the irrigated northern slopes of Tianshan Mountains, Xinjiang, China. *Catena* **2021**, *206*, 105561. [CrossRef]
4. Condon, L.E.; Atchley, A.L.; Maxwell, R.M. Evapotranspiration depletes groundwater under warming over the contiguous United States. *Nat. Commun.* **2020**, *11*, 873. [CrossRef]
5. Kløve, B.; Ala-Aho, P.; Bertrand, G.; Gurdak, J.J.; Kupfersberger, H.; Kværner, J.; Muotka, T.; Mykrä, H.; Preda, E.; Rossi, P.; et al. Climate change impacts on groundwater and dependent ecosystems. *J. Hydrol.* **2014**, *518*, 250–266. [CrossRef]
6. Rohde, M.M.; Albano, C.M.; Huggins, X.; Klausmeyer, K.R.; Morton, C.; Sharman, A.; Zaveri, E.; Saito, L.; Freed, Z.; Howard, J.K.; et al. Groundwater-dependent ecosystem map exposes global dryland protection needs. *Nature* **2024**, *632*, 101–107. [CrossRef]
7. Nan, Y.; Huo, J.; Han, G.; Hu, R.; Zhao, Y.; Zhang, Y.; Lu, X.; Zhou, Y.; Groh, J.; Zhang, Z. Groundwater Altered Water Balance and Plant Water Use Efficiency in Desert Ecosystems. *Water Resour. Res.* **2025**, *61*, e2025WR040545. [CrossRef]
8. Liu, B.; Guan, H.; Zhao, W.; Yang, Y.; Li, S. Groundwater facilitated water-use efficiency along a gradient of groundwater depth in arid northwestern China. *Agric. For. Meteorol.* **2017**, *233*, 235–241. [CrossRef]
9. Wu, H.; Zhou, P.; Song, X.; Sun, W.; Li, Y.; Song, S.; Zhang, Y. Dynamics of solar-induced chlorophyll fluorescence (SIF) and its response to meteorological drought in the Yellow River Basin. *J. Environ. Manag.* **2024**, *360*, 121023. [CrossRef]
10. Xu, Z.; Mason, J.A.; Lu, H. Vegetated dune morphodynamics during recent stabilization of the Mu Us dune field, north-central China. *Geomorphology* **2015**, *228*, 486–503. [CrossRef]
11. Cui, X.; Sun, H.; Dong, Z.; Liu, Z.; Li, C.; Zhang, Z.; Li, X.; Li, L. Temporal variation of the wind environment and its possible causes in the Mu Us Dunefield of Northern China, 1960–2014. *Theor. Appl. Climatol.* **2018**, *135*, 1017–1029. [CrossRef]
12. Huang, F.; Chunyu, X.; Zhang, D.; Chen, X.; Ochoa, C.G. A framework to assess the impact of ecological water conveyance on groundwater-dependent terrestrial ecosystems in arid inland river basins. *Sci. Total Environ.* **2020**, *709*, 136155. [CrossRef]
13. Liu, Y.; Ge, J.; Guo, W.; Cao, Y.; Chen, C.; Luo, X.; Yang, L.; Wang, S. Revisiting Biophysical Impacts of Greening on Precipitation Over the Loess Plateau of China Using WRF With Water Vapor Tracers. *Geophys. Res. Lett.* **2023**, *50*, e2023GL102809. [CrossRef]
14. Zhang, B.; Tian, L.; Yang, Y.; He, X. Revegetation Does Not Decrease Water Yield in the Loess Plateau of China. *Geophys. Res. Lett.* **2022**, *49*, e2022GL098025. [CrossRef]
15. Li, B.; Wang, X.; Li, Z. Plants extend root deeper rather than increase root biomass triggered by critical age and soil water depletion. *Sci. Total Environ.* **2024**, *914*, 169689. [CrossRef] [PubMed]
16. Etesami, H.; Chen, Y. Chapter 28–Adapting to arid conditions: The Interplay of Plant Roots, Microbial Communities, and Exudates in the Face of Drought Challenges. In *Sustainable Agriculture under Drought Stress*; Etesami, H., Chen, Y., Eds.; Academic Press: Cambridge, MA, USA, 2025; pp. 471–487. [CrossRef]
17. Liu, Q.; Zhang, Q.; Yan, Y.; Zhang, X.; Niu, J.; Svenning, J.-C. Ecological restoration is the dominant driver of the recent reversal of desertification in the Mu Us Desert (China). *J. Clean. Prod.* **2020**, *268*, 122241. [CrossRef]
18. Feng, X.; Fu, B.; Piao, S.; Wang, S.; Ciais, P.; Zeng, Z.; Lü, Y.; Zeng, Y.; Li, Y.; Jiang, X.; et al. Revegetation in China's Loess Plateau is approaching sustainable water resource limits. *Nat. Clim. Change* **2016**, *6*, 1019–1022. [CrossRef]

19. Liu, M.; Zhai, H.; Zhang, X.; Dong, X.; Hu, J.; Ma, J.; Sun, W. Time-lag and accumulation responses of vegetation growth to average and extreme precipitation and temperature events in China between 2001 and 2020. *Sci. Total Environ.* **2024**, *945*, 174084. [CrossRef]
20. He, L.; Guo, J.; Jiang, Q.; Zhang, Z.; Yu, S. How did the Chinese Loess Plateau turn green from 2001 to 2020? An explanation using satellite data. *Catena* **2022**, *214*, 106246. [CrossRef]
21. Wang, Y.; Zhang, Y.; Yu, X.; Jia, G.; Liu, Z.; Sun, L.; Zheng, P.; Zhu, X. Grassland soil moisture fluctuation and its relationship with evapotranspiration. *Ecol. Indic.* **2021**, *131*, 108196. [CrossRef]
22. Yuxi, W.; Li, P.; Yuemin, Y.; Tiantian, C. Global Vegetation-Temperature Sensitivity and Its Driving Forces in the 21st Century. *Earth's Future* **2024**, *12*, e2022EF003395. [CrossRef]
23. Shi, S.; Yang, P.; Vrieling, A.; Tol, C.V.D. Vegetation optimal temperature modulates global vegetation season onset shifts in response to warming climate. *Commun. Earth Environ.* **2025**, *6*, 203. [CrossRef]
24. Denissen, J.M.C.; Teuling, A.J.; Pitman, A.J.; Koirala, S.; Migliavacca, M.; Li, W.; Reichstein, M.; Winkler, A.J.; Zhan, C.; Orth, R. Widespread shift from ecosystem energy to water limitation with climate change. *Nat. Clim. Change* **2022**, *12*, 677–684. [CrossRef]
25. Shilong, P.; Jingyun, F.; Wei, J.; Qinghua, G.; Jinhu, K.; Shu, T. Variation in a Satellite-Based Vegetation Index in Relation to Climate in China. *J. Veg. Sci.* **2004**, *15*, 219–226. [CrossRef]
26. Lv, J.; Wang, X.S.; Zhou, Y.; Qian, K.; Wan, L.; Eamus, D.; Tao, Z. Groundwater-dependent distribution of vegetation in Hailiutu River catchment, a semi-arid region in China. *Ecohydrology* **2012**, *6*, 142–149. [CrossRef]
27. Krause, S.; Hannah, D.M.; Sadler, J.P.; Wood, P.J. Ecohydrology on the edge: Interactions across the interfaces of wetland, riparian and groundwater-based ecosystems. *Ecohydrology* **2011**, *4*, 477–480. [CrossRef]
28. Rohde, M.M.; Stella, J.C.; Singer, M.B.; Roberts, D.A.; Caylor, K.K.; Albano, C.M. Establishing ecological thresholds and targets for groundwater management. *Nat. Water* **2024**, *2*, 312–323. [CrossRef]
29. Dao, P.U.; Heuzard, A.G.; Le, T.X.H.; Zhao, J.; Yin, R.; Shang, C.; Fan, C. The impacts of climate change on groundwater quality: A review. *Sci. Total Environ.* **2024**, *912*, 169241. [CrossRef]
30. Benz, S.A.; Irvine, D.J.; Rau, G.C.; Bayer, P.; Menberg, K.; Blum, P.; Jamieson, R.C.; Griebler, C.; Kurylyk, B.L. Global groundwater warming due to climate change. *Nat. Geosci.* **2024**, *17*, 545–551. [CrossRef]
31. Murray, B.R.; Hose, G.C.; Eamus, D.; Licari, D. Valuation of groundwater-dependent ecosystems: A functional methodology incorporating ecosystem services. *Aust. J. Bot.* **2006**, *54*, 221. [CrossRef]
32. Howard, J.K.; Dooley, K.; Brauman, K.A.; Klausmeyer, K.R.; Rohde, M.M. Ecosystem services produced by groundwater dependent ecosystems: A framework and case study in California. *Front. Water* **2023**, *5*, 1115416. [CrossRef]
33. He, Q.; Wang, M.; Liu, K.; Wang, B. High-resolution Standardized Precipitation Evapotranspiration Index (SPEI) reveals trends in drought and vegetation water availability in China. *Geogr. Sustain.* **2025**, *6*, 100228. [CrossRef]
34. Lu, Y.; Yang, T.; Fu, J.; Song, W. Utility of the standardized precipitation evapotranspiration index (SPEI) to detect agricultural droughts over China. *J. Hydrol. Reg. Stud.* **2025**, *58*, 102190. [CrossRef]
35. Dong, J.; Zhang, J.; Gu, X.; Gao, H.; Yang, B.; Yang, X.; Zhao, C.; Zhang, T.; Yin, L.; Wang, X. Groundwater dependent ecosystems assessment in catchment scale of semi-arid regions: A case study in the Hailiutu catchment of the Ordos Plateau. *Geol. China* **2024**, *51*, 1855–1867.
36. Yang, Z.; Zhou, Y.; Wenninger, J.; Uhlenbrook, S.; Wang, X.; Wan, L. Groundwater and surface-water interactions and impacts of human activities in the Hailiutu catchment, northwest China. *Hydrogeol. J.* **2017**, *25*, 1341–1355. [CrossRef]
37. Zhou, Y.; Wenninger, J.; Yang, Z.; Yin, L.; Huang, J.; Hou, L.; Wang, X.; Zhang, D.; Uhlenbrook, S. Groundwater–surface water interactions, vegetation dependencies and implications for water resources management in the semi-arid Hailiutu River catchment, China – a synthesis. *Hydrol. Earth Syst. Sci.* **2013**, *17*, 2435–2447. [CrossRef]
38. Jin, X.M.; Guo, R.H.; Zhang, Q.; Zhou, Y.X.; Zhang, D.R.; Yang, Z. Response of vegetation pattern to different landform and water-table depth in Hailiutu River basin, Northwestern China. *Environ. Earth Sci.* **2014**, *71*, 4889–4898. [CrossRef]
39. Wang, T.; Wu, Z.; Wang, P.; Wu, T.; Zhang, Y.; Yin, J.; Yu, J.; Wang, H.; Guan, X.; Xu, H.; et al. Plant-groundwater interactions in drylands: A review of current research and future perspectives. *Agric. For. Meteorol.* **2023**, *341*, 109636. [CrossRef]
40. Shao, G.; Guan, Y.; Zhang, D.; Yu, B.; Zhu, J. The Impacts of Climate Variability and Land Use Change on Streamflow in the Hailiutu River Basin. *Water* **2018**, *10*, 814. [CrossRef]
41. Save, H.; Bettadpur, S.; Tapley, B.D. High-resolution CSR GRACE RL05 mascons. *J. Geophys. Res. Solid Earth* **2016**, *121*, 7547–7569. [CrossRef]
42. Save, H. *CSR GRACE and GRACE-FO RL06 Mascon Solutions v02*; University of Texas at Austin: Austin, TX, USA, 2020; p. 1.
43. Liu, P.-W.; Famiglietti, J.S.; Purdy, A.J.; Adams, K.H.; McEvoy, A.L.; Reager, J.T.; Bindlish, R.; Wiese, D.N.; David, C.H.; Rodell, M. Groundwater depletion in California's Central Valley accelerates during megadrought. *Nat. Commun.* **2022**, *13*, 7825. [CrossRef] [PubMed]

44. Zhang, G.; Xu, T.; Yin, W.; Bateni, S.M.; Jun, C.; Kim, D.; Liu, S.; Xu, Z.; Ming, W.; Wang, J. A machine learning downscaling framework based on a physically constrained sliding window technique for improving resolution of global water storage anomaly. *Remote Sens. Environ.* **2024**, *313*, 114359. [CrossRef]
45. Fernandes, R.; Leblanc, S.G. Parametric (modified least squares) and non-parametric (Theil–Sen) linear regressions for predicting biophysical parameters in the presence of measurement errors. *Remote Sens. Environ.* **2005**, *95*, 303–316. [CrossRef]
46. Sen, P.K. Estimates of the Regression Coefficient Based on Kendall's Tau. *J. Am. Stat. Assoc.* **1968**, *63*, 1379–1389. [CrossRef]
47. Meng, S.; Xie, X.; Zhu, B.; Wang, Y. The relative contribution of vegetation greening to the hydrological cycle in the Three-North region of China: A modelling analysis. *J. Hydrol.* **2020**, *591*, 125689. [CrossRef]
48. Yang, L.; Wei, W.; Chen, L.; Chen, W.; Wang, J. Response of temporal variation of soil moisture to vegetation restoration in semi-arid Loess Plateau, China. *Catena* **2014**, *115*, 123–133. [CrossRef]
49. Mann, H.B. Nonparametric Tests Against Trend. *Econometrica* **1945**, *13*, 245–259. [CrossRef]
50. Isabona, J.; Imoize, A.L.; Kim, Y. Machine Learning-Based Boosted Regression Ensemble Combined with Hyperparameter Tuning for Optimal Adaptive Learning. *Sensors* **2022**, *22*, 3776. [CrossRef]
51. Wang, Y.; Chen, X.; Gao, M.; Dong, J. The use of random forest to identify climate and human interference on vegetation coverage changes in southwest China. *Ecol. Indic.* **2022**, *144*, 109463. [CrossRef]
52. Chan, J.C.-W.; Paelinckx, D. Evaluation of Random Forest and Adaboost tree-based ensemble classification and spectral band selection for ecotope mapping using airborne hyperspectral imagery. *Remote Sens. Environ.* **2008**, *112*, 2999–3011. [CrossRef]
53. Zhang, X.; Shen, H.; Huang, T.; Wu, Y.; Guo, B.; Liu, Z.; Luo, H.; Tang, J.; Zhou, H.; Wang, L.; et al. Improved random forest algorithms for increasing the accuracy of forest aboveground biomass estimation using Sentinel-2 imagery. *Ecol. Indic.* **2024**, *159*, 111752. [CrossRef]
54. Lu, F.; Zhang, G.; Wang, T.; Ye, Y.; Zhao, Q. Geographically Weighted Random Forest Based on Spatial Factor Optimization for the Assessment of Landslide Susceptibility. *Remote Sens.* **2025**, *17*, 1608. [CrossRef]
55. Medina, B.L.; Carey, L.D.; Amiot, C.G.; Mecikalski, R.M.; Roeder, W.P.; McNamara, T.M.; Blakeslee, R.J. A Random Forest Method to Forecast Downbursts Based on Dual-Polarization Radar Signatures. *Remote Sens.* **2019**, *11*, 826. [CrossRef]
56. Fildes, S.G.; Doody, T.M.; Bruce, D.; Clark, I.F.; Batelaan, O. Mapping groundwater dependent ecosystem potential in a semi-arid environment using a remote sensing-based multiple-lines-of-evidence approach. *Int. J. Digit. Earth* **2023**, *16*, 375–406. [CrossRef]
57. Bai, T.; Wang, X.-S.; Han, P.-F. Controls of groundwater-dependent vegetation coverage in the yellow river basin, china: Insights from interpretable machine learning. *J. Hydrol.* **2024**, *631*, 130747. [CrossRef]
58. Huang, R.; Luo, W.; Liu, Y.; Wang, J.; Zhang, L. Spatiotemporal Variations and Driving Mechanisms of Vegetation Phenology Across Different Vegetation Types in Yan Mountain from 2000 to 2022. *Remote Sens.* **2025**, *17*, 3051. [CrossRef]
59. Ren, H.; Wen, Z.; Liu, Y.; Lin, Z.; Han, P.; Shi, H.; Wang, Z.; Su, T. Vegetation response to changes in climate across different climate zones in China. *Ecol. Indic.* **2023**, *155*, 110932. [CrossRef]
60. Wang, F.; Zhang, Z.; Du, M.; Lu, J.; Chen, X. Drought Amplifies the Suppressive Effect of Afforestation on Net Primary Productivity in Semi-Arid Ecosystems: A Case Study of the Yellow River Basin. *Remote Sens.* **2025**, *17*, 2100. [CrossRef]
61. Chen, Z.; Qin, H.; Zhang, X.; Xue, H.; Wang, S.; Zhang, H. The Impact of Meteorological Drought at Different Time Scales from 1986 to 2020 on Vegetation Changes in the Shendong Mining Area. *Remote Sens.* **2024**, *16*, 2843. [CrossRef]
62. Jiao, W.; Wang, L.; Smith, W.K.; Chang, Q.; Wang, H.; D'Odorico, P. Observed increasing water constraint on vegetation growth over the last three decades. *Nat. Commun.* **2021**, *12*, 3777. [CrossRef]
63. Gao, S.; Lü, Y.; Jiang, X. Increased precipitation and vegetation cover synergistically enhanced the availability and effectiveness of water resources in a dryland region. *J. Hydrol.* **2025**, *654*, 132812. [CrossRef]
64. Wang, C.; Cui, A.; Ji, R.; Huang, S.; Li, P.; Chen, N.; Shao, Z. Spatiotemporal Responses of Global Vegetation Growth to Terrestrial Water Storage. *Remote Sens.* **2025**, *17*, 1701. [CrossRef]
65. Delgado-Baquerizo, M.; Eldridge, D.J.; Feng, Y.; Zhang, J.; Guirado, E. Highly protected areas buffer against aridity thresholds in global drylands. *Nat. Plants* **2025**, *11*, 2041–2049. [CrossRef] [PubMed]
66. Belgrano, A.; Cucchiella, F.; Jiang, D.; Rotilio, M. Anthropogenic modifications: Impacts and conservation strategies. *Sci. Rep.* **2023**, *13*, 12009. [CrossRef]
67. Zheng, K.; Tan, L.; Sun, Y.; Wu, Y.; Duan, Z.; Xu, Y.; Gao, C. Impacts of climate change and anthropogenic activities on vegetation change: Evidence from typical areas in China. *Ecol. Indic.* **2021**, *126*, 107648. [CrossRef]
68. Chen, H.; Fan, L.; Li, Q.; Wang, Y.; Liu, D.; Zhao, F. Future climate change exacerbates streamflow depletion in the Wei River Basin, China. *J. Hydrol.* **2025**, *663*, 134146. [CrossRef]
69. Jasechko, S.; Seybold, H.; Perrone, D.; Fan, Y.; Shamsudduha, M.; Taylor, R.G.; Fallatah, O.; Kirchner, J.W. Rapid groundwater decline and some cases of recovery in aquifers globally. *Nature* **2024**, *625*, 715–721. [CrossRef]
70. Abbas, S.A.; Bailey, R.T.; White, J.T.; Arnold, J.G.; White, M.J. Estimation of groundwater storage loss using surface–subsurface hydrologic modeling in an irrigated agricultural region. *Sci. Rep.* **2025**, *15*, 8350. [CrossRef]

71. Stocker, B.D.; Tumber-Dávila, S.J.; Konings, A.G.; Anderson, M.C.; Hain, C.; Jackson, R.B. Global patterns of water storage in the rooting zones of vegetation. *Nat. Geosci.* **2023**, *16*, 250–256. [CrossRef]
72. Carroll, R.W.H.; Niswonger, R.G.; Ulrich, C.; Varadharajan, C.; Siirila-Woodburn, E.R.; Williams, K.H. Declining groundwater storage expected to amplify mountain streamflow reductions in a warmer world. *Nat. Water* **2024**, *2*, 419–433. [CrossRef]
73. Chen, H.; Liu, J.; He, W.; Xu, P.; Nguyen, N.T.; Lv, Y.; Huang, C. Shifted vegetation resilience from loss to gain driven by changes in water availability and solar radiation over the last two decades in Southwest China. *Agric. For. Meteorol.* **2025**, *368*, 110543. [CrossRef]
74. Zhou, D.; Zheng, C.; Jia, L.; Menenti, M.; Lu, J.; Chen, Q. Evaluating the Performance of Irrigation Using Remote Sensing Data and the Budyko Hypothesis: A Case Study in Northwest China. *Remote Sens.* **2025**, *17*, 1085. [CrossRef]
75. Wang, L.; Yue, Y.; Cui, J.; Liu, H.; Shi, L.; Liang, B.; Li, Q.; Wang, K. Precipitation sensitivity of vegetation growth in southern China depends on geological settings. *J. Hydrol.* **2024**, *643*, 131916. [CrossRef]
76. Cui, J.; Lian, X.; Huntingford, C.; Gimeno, L.; Wang, T.; Ding, J.; He, M.; Xu, H.; Chen, A.; Gentine, P.; et al. Global water availability boosted by vegetation-driven changes in atmospheric moisture transport. *Nat. Geosci.* **2022**, *15*, 982–988. [CrossRef]
77. Shi, J.; Liu, M.; Li, Y.; Guan, C. Response of total primary productivity of vegetation to meteorological drought in arid and semi-arid regions of China. *J. Arid Environ.* **2025**, *228*, 105346. [CrossRef]
78. Zhang, S.; Li, J.; Zhang, T.; Feng, P.; Liu, W. Response of vegetation to SPI and driving factors in Chinese mainland. *Agric. Water Manag.* **2024**, *291*, 108625. [CrossRef]
79. Du, Y.; Lv, S.; Wang, F.; Xu, J.; Zhao, H.; Tang, L.; Wang, H.; Zhang, H. Investigation into the temporal impacts of drought on vegetation dynamics in China during 2000 to 2022. *Sci. Rep.* **2025**, *15*, 6351. [CrossRef]
80. Jia, X.; O'Connor, D.; Hou, D.; Jin, Y.; Li, G.; Zheng, C.; Ok, Y.S.; Tsang, D.C.W.; Luo, J. Groundwater depletion and contamination: Spatial distribution of groundwater resources sustainability in China. *Sci. Total Environ.* **2019**, *672*, 551–562. [CrossRef]
81. Hu, Y.; Li, H.; Wu, D.; Chen, W.; Zhao, X.; Hou, M.; Li, A.; Zhu, Y. LAI-indicated vegetation dynamic in ecologically fragile region: A case study in the Three-North Shelter Forest program region of China. *Ecol. Indic.* **2021**, *120*, 106932. [CrossRef]
82. Deng, Y.; Wang, S.; Bai, X.; Luo, G.; Wu, L.; Chen, F.; Wang, J.; Li, C.; Yang, Y.; Hu, Z.; et al. Vegetation greening intensified soil drying in some semi-arid and arid areas of the world. *Agric. For. Meteorol.* **2020**, *292*, 108103. [CrossRef]
83. Fang, X.; Zhao, W.; Wang, L.; Feng, Q.; Ding, J.; Liu, Y.; Zhang, X. Variations of deep soil moisture under different vegetation types and influencing factors in a watershed of the Loess Plateau, China. *Hydrol. Earth Syst. Sci.* **2016**, *20*, 3309–3323. [CrossRef]
84. Scanlon, B.R.; Fakhreddine, S.; Rateb, A.; de Graaf, I.; Famiglietti, J.; Gleeson, T.; Grafton, R.Q.; Jobbagy, E.; Kebede, S.; Kolusu, S.R.; et al. Global water resources and the role of groundwater in a resilient water future. *Nat. Rev. Earth Environ.* **2023**, *4*, 87–101. [CrossRef]
85. Rowland, J.A.; Nicholson, E.; Ferrer-Paris, J.R.; Keith, D.A.; Murray, N.J.; Sato, C.F.; Tóth, A.B.; Tolsma, A.; Venn, S.; Asmüssen, M.V.; et al. Assessing risk of ecosystem collapse in a changing climate. *Nat. Clim. Change* **2025**, *15*, 597–609. [CrossRef]
86. Huggins, X.; Gleeson, T.; Serrano, D.; Zipper, S.; Jehn, F.; Rohde, M.M.; Abell, R.; Vigerstol, K.; Hartmann, A. Overlooked risks and opportunities in groundwatersheds of the world's protected areas. *Nat. Sustain.* **2023**, *6*, 855–864. [CrossRef]
87. Rodell, M.; Velicogna, I.; Famiglietti, J.S. Satellite-based estimates of groundwater depletion in India. *Nature* **2009**, *460*, 999–1002. [CrossRef]
88. Kundzewicz, Z.W.; DÖLl, P. Will groundwater ease freshwater stress under climate change? *Hydrol. Sci. J.* **2009**, *54*, 665–675. [CrossRef]
89. Pritchett, D.; Manning, S.J. Response of an Intermountain Groundwater-Dependent Ecosystem to Water Table Drawdown. *West. North Am. Nat.* **2012**, *72*, 48–59. [CrossRef]
90. Rohde, M.M.; Biswas, T.; Housman, I.W.; Campbell, L.S.; Klausmeyer, K.R.; Howard, J.K. A Machine Learning Approach to Predict Groundwater Levels in California Reveals Ecosystems at Risk. *Front. Earth Sci.* **2021**, *9*. [CrossRef]

Disclaimer/Publisher's Note: The statements, opinions and data contained in all publications are solely those of the individual author(s) and contributor(s) and not of MDPI and/or the editor(s). MDPI and/or the editor(s) disclaim responsibility for any injury to people or property resulting from any ideas, methods, instructions or products referred to in the content.